Quaternary Science Reviews 219 (2019) 112–125

Contents lists available at ScienceDirect

Quaternary Science Reviews

journal homepage: www.elsevier.com/locate/quascirev

Holocene sea levels in Southeast Asia, Maldives, India and Sri Lanka: The SEAMIS database

Thomas Mann [a, *], Maren Bender [a, b], Thomas Lorscheid [a, b], Paolo Stocchi [c], Matteo Vacchi [d], Adam D. Switzer [e, f], Alessio Rovere [a, b]

[a] Leibniz Centre for Tropical Marine Research (ZMT), Fahrenheitstraße 6, 28359, Bremen, Germany
[b] University of Bremen, Center for Marine Environmental Sciences (MARUM), Leobener Straße 8, 28359, Bremen, Germany
[c] NIOZ Royal Netherlands Institute for Sea Research, Department of Coastal Systems, Utrecht University, Den Horn, Texel, the Netherlands
[d] Geography, College of Life and Environmental Sciences, University of Exeter, EX4 4RJ, Exeter, UK
[e] Asian School of the Environment, Nanyang Technological University, Singapore, 649812, Singapore
[f] Earth Observatory of Singapore, Nanyang Technological University, Singapore, 649812, Singapore

ARTICLE INFO

Article history:
Received 17 February 2018
Received in revised form
6 July 2019
Accepted 7 July 2019
Available online 18 July 2019

Keywords:
Glacial isostatic adjustment
Sea-level highstand
Sea-level rise
Climate change
Tectonics

ABSTRACT

We assembled a database of Holocene relative sea-level index points (n = 213) and marine (n = 211) and terrestrial (n = 122) limiting points for the broader South and Southeast Asian region including the Maldives, India and Sri Lanka. The standardized review of published age-elevation information from corals, deltaic, estuarine and mangrove deposits, beachrocks and tidal notches, yielded a new suite of relative sea-level index and limiting points produced according to a standardized protocol. Expected spatial variability in Holocene relative sea-level change due to glacial isostatic adjustment was accounted for, by first subdividing the study area into ten geographic sub-regions from the Central Indian Ocean to the Western Tropical Pacific, and second by comparing sub-regional relative sea-level data to model predictions of glacial isostatic adjustment. Results show that some of the regionally constrained relative sea-level data are characterized by significant inconsistencies that cannot be explained by glacial isostatic adjustment. Such inconsistencies of standardized relative sea-level data become particularly obvious in areas around the Red River Delta in Vietnam, the Gulf of Thailand, the northwest coast of Malaysia and the Spermonde Archipelago in Indonesia. Based on a critical evaluation of the reviewed relative sea-level indicators, we discuss possible sources of local divergence and identify regions where data are currently insufficient to constrain glacial isostatic adjustment predictions. The remaining quality-controlled and consistent relative sea-level data show that glacial isostatic adjustment and syn-/post-formational influences such as tectonic uplift, subsidence and compaction were the dominant local drivers of Holocene relative sea-level change. Collectively, the results of this review suggest that Holocene sea levels in South and Southeast Asia and surrounding regions have been controlled by a variety of global and local drivers and imply that additional index points from the Java Sea in Indonesia would be valuable to better assess the spatial variability, and to calibrate geophysical models of glacial isostatic adjustment.

1. Introduction

Coastal areas in South and Southeast (SE) Asia are among the world's most vulnerable in terms of flooding due to climate induced sea-level rise and the associated land and economic loss (Nicholls and Cazenave, 2010; Cazenave and Cozannet, 2013). Throughout much of Asia, socio-economic risks primarily emerge from high rates of relative sea-level (RSL) rise in coastal megacities that are largely a product of subsidence resulting from groundwater extraction (Chaussard et al., 2013). Subsidence-driven RSL rise exacerbates the climatic signal and is most problematic in rapidly developing coastal megacities where population growth and urbanization will further increase the exposure to climate-related weather extremes and sea-level rise in the future (Hanson et al., 2011).

Located far field of ice-sheets that covered vast regions in higher and middle latitudes during the Last Glacial Maximum (LGM, ~21

* Corresponding author. Fahrenheitstraße 6, 28211, Bremen, Germany.
E-mail address: thomas.mann@leibniz-zmt.de (T. Mann).

https://doi.org/10.1016/j.quascirev.2019.07.007

ka before present, BP), deglacial RSL changes within the equatorial ocean basins of SE Asia resulted from a combination of eustatic, isostatic and local factors (Sieh et al., 2008; Mann et al., 2016; Meltzner et al., 2017). In contrast to near- and intermediate-field regions such as Greenland, Northern Europe and North America (Long et al., 2006; Hijma and Cohen, 2010; Engelhart and Horton, 2012; Horton et al., 2013; Engelhart et al., 2015), the Holocene RSL record in the far field is minimally influenced by isostatic deformation resulting from weight relief after the melting of thick LGM ice sheets (Shennan and Horton, 2002; Gehrels and Long, 2008). Rather, the melting of ice sheets in high-latitudinal regions induced a collapse of the peripheral forebulge, which had been surrounding the former ice margins, and thereby caused a redistribution of water masses away from the tropics and towards higher latitudes (i.e. ocean siphoning; Mitrovica and Peltier, 1991; Peltier, 1999).

As a result, a Holocene RSL highstand in equatorial ocean basins in SE Asia is predicted by geophysical models, unless the eustatic contribution and subsequent redistribution of water following the subsidence of the peripheral forebulge has been compensated by contemporaneous hydro-isostatic subsidence of the oceanic crust (i.e. continental levering; Lambeck et al., 2002; Mitrovica and Milne, 2002; Lambeck et al., 2010; Woodroffe et al., 2012). The interplay between these processes (i.e. ocean siphoning and hydro-isostasy/continental levering) predominantly determines glacial isostatic adjustment (GIA) patterns in equatorial ocean basins. Furthermore, in regions such as South and SE Asia, the possibility of tectonically-induced, post-formational changes in the elevation of RSL indicators is often relevant, potentially adding additional uncertainty to the interpretation of reconstructions.

Regional sea-level databases summarizing RSL index and limiting points since the LGM provide meaningful insights to disentangle the primary driving mechanisms of RSL change and its potential environmental and societal impacts (e.g. Love et al., 2016; Yousefi et al., 2018). Accurate and precise RSL reconstructions are essential to understand variability in Earth's rheology (Engelhart et al., 2011; Roy and Peltier, 2015), identify ice-volume equivalent melt-water contributions (Lambeck et al., 2014; Bradley et al., 2016) and to reconstruct shoreline responses to RSL changes as a valuable benchmark against which to assess modern and ancient hominin dispersals (Lambeck and Chappell, 2001; Carto et al., 2009; Armitage et al., 2011; Fontana et al., 2017; Melis et al., 2018).

In SE Asia, RSL studies summarizing some of the hitherto existing deglacial RSL data from within this region, as well as from the broader Indo-Pacific region are provided by Horton et al. (2005) for the Malay-Thai Peninsula and Woodroffe and Horton (2005). For example, Horton et al. (2005) analyzed the facies of ancient mangrove and freshwater swamps in the Great Songkhla Lakes at the southwest coast of Thailand, and compared their results to earlier RSL reconstructions from the Malay-Thai Peninsula. In this region, they identified strong spatial variability of RSL signals across the study sites culminating in a maximum mid-Holocene highstand of ~5 m above present-day mean sea level (msl) by ~ 4.9–4.5 ka BP. The spatial spread of Holocene RSL variability is explained by regional differences in the hydro-isostatic response of the ocean floor affecting the RSL signal in that area. Such datasets therefore provide valuable contributions to the growing awareness of Holocene sea-level variability, and, at the same time, call for an updated, quality-controlled and standardized framework summarizing the spatial and temporal variability of Holocene RSL change for the broader SE Asian region.

In this paper, we have standardized data from terrestrial, intertidal and marine deposits into 546 RSL index and limiting points from ten regions within South and SE Asia, including the Indo – West Pacific. To produce the RSL data points along with their associated uncertainty, we followed the protocols described by International Geoscience Correlation Programme (IGCP) projects 61, 200, 495, 588, and 639 (e.g. Preuss, 1979; Van de Plassche, 1986; Gehrels and Long, 2008; Horton et al., 2009; Shennan et al., 2015). Our results represent the first standardized Holocene RSL database for broader SE Asia, Maldives, India and Sri Lanka (hereafter abbreviated to SEAMIS). The new SEAMIS dataset allows for an examination of driving mechanisms of RSL change within individual sub-regions as well as the identification of those areas where additional focussed efforts to produce high-quality RSL data are required.

2. Regional setting

2.1. Geography

SE Asia is a vast geographic zone comprising countries located on the southeastern extension of continental Asia (Myanmar, Thailand, Laos, Cambodia, Vietnam, Malaysia, Singapore), the island of Borneo (comprising Brunei and parts of Indonesia and Malaysia) and the archipelagos of Indonesia and the Philippines. In the SEAMIS dataset, we have furthermore included RSL studies from the Maldives (Kench et al., 2009) and Cocos (Keeling) Islands (Woodroffe et al., 1990) in the central and eastern Indian Ocean, southeastern India (Vaz and Banerjee, 1997; Banerjee, 2000), the Palau Islands in the western tropical Pacific (Kayanne et al., 2002) and the Huon Peninsula, Papua New Guinea (Chappell and Polach, 1991). This results in a geographical extension of the study area ranging between 20°N and 20°S latitudes and 70°E–150°E longitudes (Fig. 1).

2.2. Tectonics

The geographic region of this study is in many parts characterized by active tectonics, which have shaped the regional geomorphology through earth history and continue to influence the behavior of the lithosphere today (Hall and Blundell, 1996; McCaffrey, 1996; Simons et al., 2007; Hall and Spakman, 2015) and inherently affect records of Holocene RSL change. The study area comprises approximately 20 different tectonic plates and microplates and an accordingly high number of plate boundaries (Bird, 2003, Fig. 1). If considered in terms of absolute length within the study area, the dominant structural units delineating the different plates from each other are subduction zones, followed by divergent plate boundaries and transform faults. For example, along the Sunda Megathrust, the Australian Plate is subducted beneath the Sunda and Timor plates and have thereby created a volcanic arc comprising the Indonesian islands of Sumatra, Java and Nusa Tenggara (Darman and Sidi, 2000). In the SEAMIS database, we exclude areas where tectonic variability represents a first-order control on RSL change (e.g., south coast of Sumatra and Java and much of the Philippines).

2.3. Climate

Located between 20°N and 20°S latitudes (Fig. 1), virtually all countries in the study area experience tropical to sub-tropical climates with predictable reversals in monsoon wind directions and associated changes between wet and dry seasons. As reefs and mangrove environments cover large parts of the coastal landscape of the region, RSL indicators that have been included in this database are dominated by corals and sediment from mangrove swamp deposits.

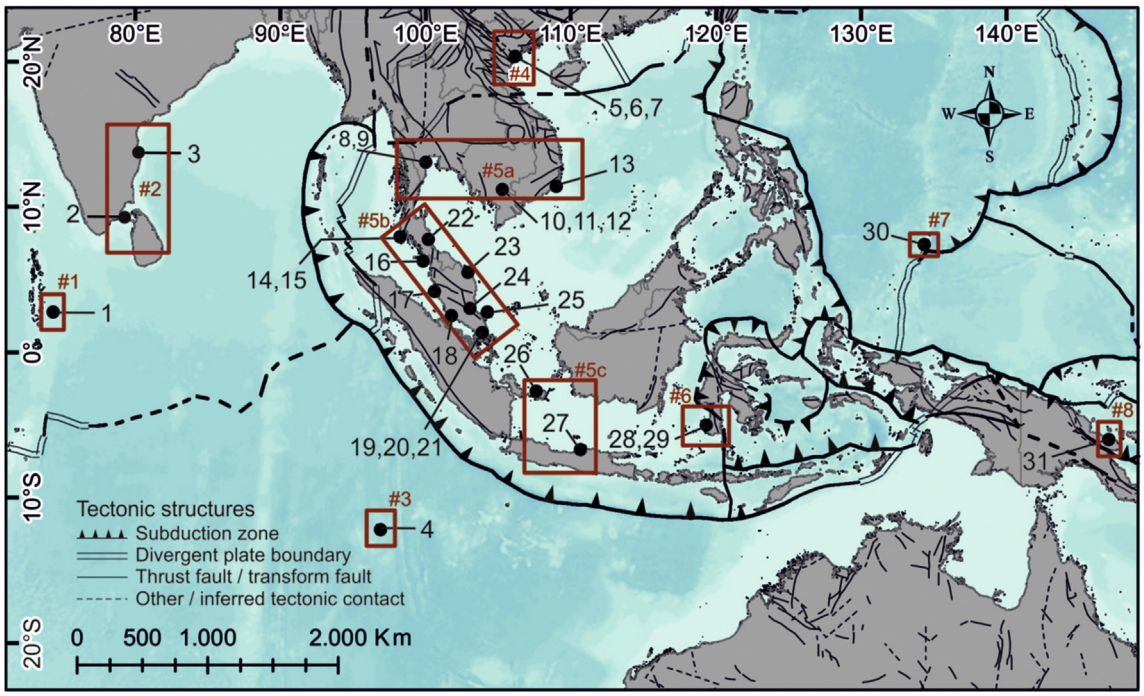

Fig. 1. Overview map of the broader SE Asian region showing the study sites of published RSL reconstructions implemented in this paper. Black numbers refer to studies listed in Table 1. Red rectangles and numbered hashtags indicate the positions of geographical sub-regions. (For interpretation of the references to color in this figure legend, the reader is referred to the Web version of this article.)

3. Material and methods

3.1. Studies reviewed and types of sea-level indicators

Sea-level changes in SE Asia have been studied since the 1970s (e.g. Tjia et al., 1972). Most RSL indicators that have been analyzed are of biological origin such as coral reefs and microatolls (e.g. Chappell and Polach, 1991; Hesp et al., 1998; Kayanne et al., 2002; Mann et al., 2016; Meltzner et al., 2017), or result from the partial decay of plant material and leaf litter that accumulate in peatlands and mangrove swamps (Geyh et al., 1979; Horton et al., 2005). Other RSL indicators are preserved within beach deposits (Stattegger et al., 2013) and deltas (Hori et al., 2004; Tamura et al., 2009), or are reconstructed from geomorphic features such as tidal notches (Scheffers et al., 2012). Table 1 summarizes all studies from which data have been incorporated to the SEAMIS database and gives the locations of the respective study sites.

3.2. Compilation of the dataset

The criteria to compile a standardized dataset of sea-level index and limiting points has been primarily described and formalized during the International Geological Correlation Program (IGCP) Project 61 (Bloom, 1977; van de Plassche, 1982) and was subsequently refined in the follow-up IGCP projects 200, 274, 367, 437, 495 and 588 (Van de Plassche, 1986; Pluet and Pirazzoli, 1991; Shennan, 1992; Murray-Wallace and Scott, 1999; Hopley and Gehrels, 2007; Gehrels and Long, 2008; Switzer et al., 2012). Most of these earlier works have been recently summarized by Shennan et al. (2015), stating that four fundamental criteria need to be reported for any index point in a standardized way (Hijma et al., 2015):

(1) elevation measurements need to be undertaken using high-precision topographic survey techniques where the obtained results can be benchmarked to a tidal datum;
(2) for every sea-level index point, the Indicative Meaning (IM), comprising the Indicative Range (IR) and the Reference Water Level (RWL), need to be calculated. IR represents the elevation range occupied by a sea-level index point relative to contemporary tidal datums. The RWL is the midpoint of the IR. Accordingly, the smaller the IR of a certain sea-level index point, the lower its vertical uncertainty in the final RSL reconstruction;
(3) the age of a sea-level index point must be obtained using radiometric dating techniques and in the case of ^{14}C dating, calibrated to take into account the variation of radiocarbon activity in the ocean and atmosphere over time;
(4) the location of a sea-level index point must be determined relative to national or international conventions.

3.3. Reconstructions of relative sea-level positions

To standardize the RSL positions obtained from the literature and apply the aforementioned criteria, we have critically reviewed published RSL evidence and allocated each RSL indicator with an IR and a RWL (Table 2).

If the IR for a given RSL indicator falls within the tidal range, then it is considered a RSL index point. RSL index points provide upper and lower limits of the elevation of RSL positions at a given time (Van de Plassche, 1986; Shennan and Horton, 2002; Engelhart et al., 2015; Shennan et al., 2015). For example, mangrove swamp deposits interpreted from sedimentological information, micro- and macrofossils and pollen assemblages (e.g. Horton et al., 2005; Bird et al., 2007; Engelhart et al., 2007; Tam et al., 2018) have been given an IR between Highest Astronomical Tide (HAT) and Mean Tide Level (MTL). Furthermore, if the information provided in the

Table 1
Summary of reviewed RSL studies and respective locations within SE Asia.

Map reference	Literature reference	Geographic subregion (map reference #)	Latitude[a]	Longitude[a]
1	Kench et al. (2009)	Central Indian Ocean (#1)	5.19	73.00
2	Banerjee (2000)	Southeastern India (#2)	9.29	79.22
3	Vaz and Banerjee (1997)	Southeastern India (#2)	13.75	80.21
4	Woodroffe et al., 1990	Eastern Indian Ocean (#3)	−11.83	96.82
5	Hori et al. (2004)	Red River Delta (#4)	20.68	105.90
6	Tanabe et al. (2003a)	Red River Delta (#4)	20.37	106.15
7	Tanabe et al. (2003b)	Red River Delta (#4)	20.63	105.99
8	Somboon and Thiramongkol (1992)	Gulf of Thailand (#5a)	14.34	100.96
9	Somboon (1988)	Gulf of Thailand (#5a)	13.50	100.50
10	Tamura et al. (2007)	South China Sea (#5a)	11.48	105.12
11	Tamura et al. (2009)	South China Sea (#5a)	11.19	105.28
12	Hanebuth et al. (2012)	South China Sea (#5a)	10.75	105.71
13	Stattegger et al. (2013)	South China Sea (#5a)	11.40	109.00
14	Scheffers et al. (2012)	Malay-Thai-Peninsula (#5b)	7.92	98.24
15	Scoffin and Le Tissier (1998)	Malay-Thai-Peninsula (#5b)	7.75	98.42
16	Tjia et al. (1972)	Malay-Thai-Peninsula (#5b)	6.28	99.82
17	Tjia and Fujii, 1992	Malay-Thai-Peninsula (#5b)	4.18	100.60
18	Geyh et al. (1979)	Malay-Thai-Peninsula (#5b)	2.52	101.77
19	Hesp et al. (1998)	Malay-Thai-Peninsula (#5b)	1.33	103.75
20	Bird et al. (2007)	Malay-Thai-Peninsula (#5b)	1.34	103.89
21	Bird et al. (2010)	Malay-Thai-Peninsula (#5b)	1.31	103.89
22	Horton et al. (2005)	Malay-Thai-Peninsula (#5b)	7.75	100.17
23	Parham et al. (2014)	Malay-Thai-Peninsula (#5b)	5.49	102.89
24	Kamaludin (2001)	Malay-Thai-Peninsula (#5b)	3.00	103.25
25	Tjia et al. (1983)	Malay-Thai-Peninsula (#5b)	2.75	104.25
26	Meltzner et al. (2017)	Java Sea (#5c)	−3.23	108.08
27	Azmy et al. (2010)	Java Sea (#5c)	−7.61	110.71
28	Mann et al. (2016)	Strait of Makassar (#6)	−5.04	119.33
29	De Klerk, 1982	Strait of Makassar (#6)	−5.59	119.49
30	Kayanne et al. (2002)	Western Tropical Pacific (#7)	7.37	134.38
31	Chappell and Polach (1991)	Huon Peninsula (#8)	−6.00	147.05

[a] Decimal degrees.

Table 2
Derivation of the indicative meanings for different indicator types implemented in this paper to calculate RSL positions for the SEAMIS database. Highest astronomical tide (HAT), mean tide level (MTL), mean higher high water (MHHW), mean lower low water (MLLW) and lowest astronomical tide (LAT).

Sample type	Evidence	Reference Water Level	Indicative Range
Index points			
Mangrove swamp	Sedimentological information and plant macrofossils referring to a general marsh environment (Hesp et al., 1998; Bird et al., 2007). Foraminiferal, diatom and pollen assemblages dominated by swamp taxa (Kamaludin, 2001; Engelhart et al., 2007; Horton et al., 2007; Tam et al., 2018).	(HAT to MTL)/2	HAT to MTL
Mangrove upper swamp	Sedimentological information and plant macrofossils referring to a high swamp environment (Horton et al., 2005; Tam et al., 2018).	(HAT to MHHW)/2	HAT to MHHW
Tidal beach	Clayey fine sand with silt beds, fining or coarsening upward, few organic spots, few foraminifers and shell fragments (Hanebuth et al., 2012).	(HAT to MHHW)/2	HAT to MHHW
Intertidal beachrock	Inter-granular aragonitic or high-magnesium calcite cements and sedimentary architecture characterized by seaward-dipping parallel lamination (Michelli, 2008; Stattegger et al., 2013; Mauz et al., 2015).	(HAT to MLLW)/2	HAT to MLLW
Intertidal mudflat	Sedimentary facies consisting of laminated sand with mud drapes and low-angle bi-directional cross-lamination (Tamura et al., 2009).	(HAT to LAT)/2	HAT to LAT
Microatoll (Individual, not ponded)	Discoid-shaped reef-flat corals with flat 'dead' upper surface and 'living' polyps around the perimeter (Scoffin and Stoddart, 1978; Smithers and Woodroffe, 2000).	(MLW to LAT)/2	MLW to LAT
Microatoll (Individual, ponded)	Microatolls for which ponding cannot be excluded (Scoffin and Stoddart, 1978).	(MHWN to LAT)/2	MHWN to LAT
Microatoll (Highest level of survival)	Diedowns identified from slabbed and x-rayed specimens (Meltzner and Woodroffe, 2015; Meltzner et al., 2017).	(MLLW to LAT)/2	MLLW to LAT
Oyster belts	In situ belts of the oyster Saccostrea cucullata (Scheffers et al., 2012; Rovere et al., 2015).	(HAT to LAT)/2	HAT to LAT
Marine limiting	Subtidal beachrock. Inter-granular, aragonitic or high-magnesium calcite cements and trough-cross stratification (Stattegger et al., 2013; Mauz et al., 2015). In situ corals. Reef and fore-reef corals identified up to genus level in cores or in outcrops (Yokoyama and Esat, 2015). Marine shells without species description and microfossil assemblages. Found in sandy and silty sediments typical of mudflat, lagoonal, upper shoreface, prodelta or marine environments, or attached to hard substrates (Tamura et al., 2009). In situ corals. Considered marine limiting if no microatoll structure is clearly described.	LAT	Below LAT
Terrestrial limiting	Backshore deposits. Landward-dipping parallel sediment lamination and beach ridges (Michelli, 2008; Stattegger et al., 2013) Limnological sediments. Plant macrofossils and microfossil assemblages typical for freshwater environments (Hesp et al., 1998; Hori et al., 2004; Tamura et al., 2009).	HAT	Above HAT

literature (i.e., text, figures and profiles) was sufficient to allocate the dated facies to an upper mangrove swamp environment, the IR is therefore better constrained to HAT to Mean Higher High Water (MHHW).

On the other hand, RSL positions that could not be allocated to a tidal datum but rather have formed with certainty below Lowest Astronomical Tide (LAT) or above HAT, have been considered as marine and terrestrial limiting points (Shennan and Horton, 2002). Such data indicate that at the time of formation, RSL was above or below the elevation of the respective indicator. This category includes, for example, deposits that have formed as part of the supratidal beach or in a freshwater environment (terrestrial limiting), or are derived from in situ corals and marine shells (marine limiting).

In the database, we treated microatolls in different ways. Microatolls comprise a relatively flat annular morphology, usually with living coral polyps around their rims and dead upper surfaces (Scoffin and Stoddart, 1978; Smithers and Woodroffe, 2000; Meltzner and Woodroffe, 2015; Meltzner et al., 2017). These type of intertidal reef-flat corals have often been used to reconstruct RSL histories in tropical areas (e.g. Kench et al., 2009; Woodroffe et al., 2012; Mann et al., 2016) because the elevation of their dead top surface approximates a tidal datum that falls between Mean Low Water Springs (MLWS) and Mean Low Water Neaps (MLWN) in semidiurnal tidal systems. For microatolls that have been growing in an open reef-flat environment (i.e. that were not ponded during their lives), we used the range between LAT and Mean Low Water (MLW) as nearly equivalent substitutes for MLWS and MLWN (Table 2) because the OSU Tidal Prediction Software (see 3.2.2) does not provide estimates of the former tidal datums. If instead fossil microatolls have been subject to ponding during their lifetime, their indicative range is larger and the RWL would fall between LAT and Mean High Water Neaps (MHWN) (Scoffin and Stoddart, 1978). In the SEAMIS database, all microatolls were interpreted as non-ponded due to the descriptions in the reviewed works.

Recent studies have demonstrated that an improved resolution in RSL reconstructions can be achieved if die-downs within individual microatolls are used as RSL index points (Meltzner and Woodroffe, 2015; Meltzner et al., 2017). This requires the analyzed fossil microatolls to be surveyed, slabbed and x-rayed. In order to account for both, the newer (slabbing) and rather classic (surface surveying) interpretation of microatolls as RSL indicators, we have defined microatoll data as RSL index points with lower precision (RWL between LAT and MLW) if the surface of individual fossil colonies have been used to determine time-averaged RSL data. These data will provide a broader timeframe of RSL change where potential small-scale fluctuations due to dynamic oceanographic and steric factors might not be resolved. If, however, Holocene microatolls have been slabbed and die-downs have been identified, these have been considered as RSL index points with higher precision (RWL between LAT and MLLW) (e.g. Meltzner et al., 2017).

Due to lack of sufficient information within the original sources, some RSL data were rejected. This was the case when (i) there was no sample location mentioned, (ii) no sample elevation given, (iii) it was not possible determine a relation between the sample elevation and msl, (iv) there was no information about which specific horizon of the respective indicator has been surveyed (eventually, in that case, RSL positions have not necessarily been rejected but were commonly “downgraded” from index to limiting points), (v) no age was given, (vi) the upper bound calibrated age was older than 12 ka BP, (vii) the radiocarbon age was too young to be calibrated, or, (viii) if the original reference was not available (see Supplementary Table 1 for details on rejected data).

3.3.1. Age of RSL indicators

All radiocarbon age calibrations were done with the latest version of the software CALIB using the Marine13 curve for marine samples and the Intcal13 curve for terrestrial samples (Reimer et al., 2013). Marine reservoir corrections have been applied according to the closest available data in the Indian Ocean and Southeast Asia (Southon et al., 2002). If a study site was located evenly distant from two or more localities from which Delta-R values are known, the weighted mean and standard deviation has been used for calibration. A notable concern is the lack of a correction for isotopic fractionation for radiocarbon dates from the older literature (Stuiver and Polach, 1977; Törnqvist et al., 2015). This became a standard procedure in most radiocarbon laboratories by the late 1970s, but some have only applied fractionation corrections (e.g., normalized to −25‰ PDB) since the mid 1980s (Hijma et al., 2015). We performed a correction for $\delta^{13}C$ fractionation, and for these calculations further information about the sample age details (e.g. the lab code or whether a bulk error was added) is available in Supplementary Table 1.

U-series ages and uncertainties (±) were taken from the original sources. Reviewed ages and uncertainties are placed in a related U-series table with further information about the measured thorium isotopes or the U/Th isotope combination that was used (Supplementary Table 1).

3.3.2. Elevation of RSL indicators

RSL positions have been calculated as the height difference between the indicator elevation and RWL (Shennan and Horton, 2002) relative to local msl obtained from the OSU Tidal Prediction Software (Egbert and Erofeeva, 2002) for each geographic subregion (see section 3.4). The total vertical uncertainty associated with every RSL indicator includes any possible error related to the production of index and limiting points (Shennan and Horton, 2002; Vacchi et al., 2016). It comprises the IR and the uncertainty associated with calculating the sample altitude (Shennan and Horton, 2002), a sampling uncertainty (Hijma et al., 2015), a survey and benchmark uncertainty (Törnqvist et al., 2004; Engelhart et al., 2011) and an uncertainty associated with the modeled tidal information (Vacchi et al., 2016). We also accounted for possible post-formational changes in the position of an index point by sediment compaction from coring (which would result in lower RSL positions) by considering the original position of a sample within the surrounding substrate (i.e. basal vs. intercalated; Engelhart et al., 2015).

Such uncertainties, related to the depth of a dated sample in a core that has shortened due to different coring techniques, have been treated following the suggestions from Hijma et al. (2015) in cases where exact uncertainties have not been reported in the respective papers. Additionally, if no precise sample elevation was provided, the sample thickness uncertainty has been defined as half of the sample thickness. Details on the individual vertical uncertainties for each RSL indicator defined as index point are reported in Supplementary Table 1. The resulting total vertical upper and lower 2-sigma uncertainty is calculated as the root sum square of each individual source of uncertainty (Shennan and Horton, 2002).

3.4. Subdivision into geographical sub-regions

Holocene RSL histories are characterized by notable spatial and temporal variability, particularly with regard to the magnitudes of Holocene highstands after meltwater input decreased (e.g. Lambeck et al., 2002; Mitrovica and Milne, 2002; Lambeck et al., 2010; Woodroffe et al., 2012). For the Malay-Thai Peninsula, for

example, this was demonstrated by Horton et al. (2005). In order to account for the Holocene RSL spatial variability, we have subdivided our dataset into ten regions, based on a number of criteria such as data availability, inferred tectonic activity and homogenous GIA patterns. This minimizes the risk of potentially erroneous compilations resulting from naturally variably RSL signals due to GIA.

The Sunda Shelf, which marks the central portion of the study area, contains the majority of RSL studies included in the present dataset. This relatively shallow platform connects the South China Sea, the Gulf of Thailand and the intervening seas between Sumatra, Java and Borneo. It is the largest shelf area within the tropics and covers an area of approximately 1.8×10^6 km^2 (Hanebuth et al., 2000). During the LGM, when the global eustatic sea-level lowstand reached a maximum value of −130 m msl (Yokoyama et al., 2018), large parts of the shelf were subaerially exposed, with late-glacial flooding initiated around 14.5 ka BP (Hanebuth et al. 2000, 2011).

The Sunda block in the central part of the Sunda Shelf has recently relative tectonic stability with vertical crustal plate motions <0.1 mm/yr (Tjia, 1996) and horizontal deformation rates < 0.4 mm/yr (Simons et al., 2007). It has been widely assumed that the Sunda block was tectonically stable at least since the Pliocene/Pleistocene boundary (Simandjuntak and Barber, 1996; Tjia and Liew, 1996). New data on deformation patterns of the Sunda Shelf based on geomorphological observations and numerical simulations of coral reef growth suggest that the shelf is slowly subsiding at rates between 0.2 and 0.3 mm/yr due to long-wavelength dynamic topography (Sarr et al., 2019). Due to these comparably low deformation rates, late- and mid-Holocene RSL studies from the Sunda Shelf provide a good opportunity to constrain GIA models.

3.5. Glacial isostatic adjustment models

The primary aim of this study is to review and standardize RSL indicators in SE Asia, Maldives, India and Sri Lanka, and to assess the quality and rigor of the published datasets. For those sub-regions where the individual study sites are distributed over a large area, we use a set of GIA model predictions to examine spatial variability within a sub-region due to GIA (see section 5.1). Furthermore, RSL also records tectonic uplift/subsidence. In Mann et al. (subm.), we use robust results from those localities, where RSL is reliably constrained by index and limiting points, and where the tectonic overprint can be approximately corrected for (study sites in the Maldives, Palau Islands and Huon Peninsula), to compare these against the output of GIA models (Mann et al. subm.). Collectively, this allows us to (i) discuss the relationship of robust and corrected RSL data with the predictions, (ii) evaluate potential post-formational changes in the elevations of RSL data where tectonic influences and sediment compaction rates are unknown, and (iii) validate the GIA model parameters considered here (see section 5.2.). Details on how the model runs were performed can be found in Table 1 of Mann et al. (subm.).

4. Results

We present our results subdivided into eight geographical regions (#1 – #8), including three sub-regions (#5a - #5c), as shown in Fig. 1. Overall, we standardized 546 RSL indicators divided into 213 index points, 122 terrestrial and 211 marine limiting points. Our data spans the past 12 ka and cover RSL signals from −45 m msl to +12 m msl (Fig. 2). Detailed information on the age-elevation information of each RSL indicator as well as additional evidence such as species information or other supporting evidence for the extraction of a RSL signal from each data point can be found in Supplementary Table 1.

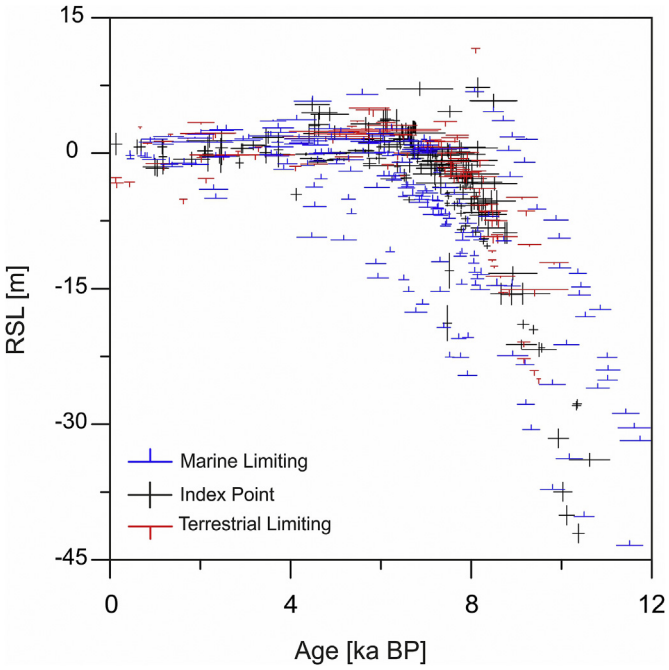

Fig. 2. Age-elevation plot of standardized Holocene RSL indicators compiled in the SEAMIS database.

4.1. Central Indian Ocean (#1)

Holocene RSL data for the central Indian Ocean originates from a study that was conducted in Hulhudhoo and Funadhoo islands, South Maalhosmadulu Atoll, Maldives by Kench et al. (2009). The dataset consists of 23 marine limiting points, obtained from three reef cores extracted from the southern Hulhudhoo reef platform, and three index points formed by in situ fossil microatolls surveyed on the reef flats of Hulhudhoo and Funadhoo (Fig. 3a). Early Holocene reefs in the central Indian Ocean initiated upward growth at ~8 ka BP when RSL was above −14 m below msl. Marine limiting points indicate a continuous rise in RSL until it reached msl for the first time at around 4.5 ka BP. The three reviewed index points from the Maldives date between 3.5 and 2.0 ka BP and place RSL a few decimeters above msl, thus providing evidence for a mid-to late-Holocene RSL Highstand in the central Indian Ocean.

4.2. Southeastern India (#2)

RSL data for the eastern and southern part of the sub-continent India are provided by Vaz and Banerjee (1997) and Banerjee (2000) and consist of one index point obtained through a peat layer and 13 marine limiting points comprising corals and marine molluscs (Fig. 3b). One RSL index point with an age of 8 ka BP lies ~4.5 m above present-day msl and it is followed by a series of marine limiting points that indicate RSL was above 1 m msl between 8 ka BP and 6 ka BP, and likely higher than 2–3 m msl between 6 ka BP and 4 ka BP. From 4 ka BP to present, RSL is constrained to above −4 m msl at 2 ka BP, and above −1.5 m msl since 2 ka BP.

4.3. Eastern Indian Ocean (#3)

The Holocene RSL history of the eastern Indian Ocean is

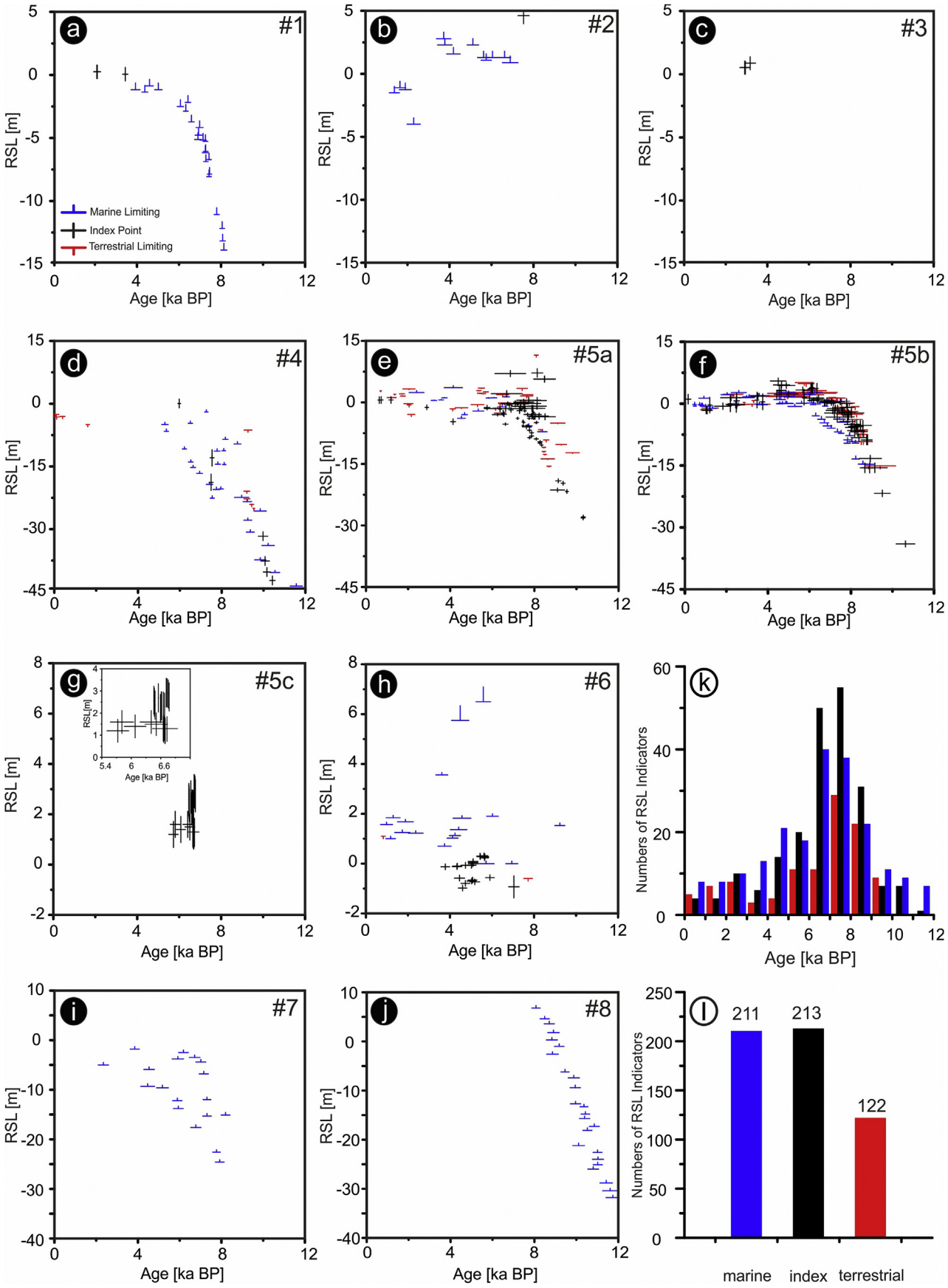

Fig. 3. Holocene RSL data for all sub-regions. a) Central Indian Ocean. b) Southeastern India. c) Eastern Indian Ocean. d) Red River Delta. e) South China Sea. f) Malay-Thai-Peninsula. g) Java Sea. h) Strait of Makassar. i) Western Tropical Pacific. j) Huon Peninsula. k) Frequency distribution of index and limiting points in the SEAMIS database. l) Histogram showing the absolute numbers of different RSL indicators implemented in the SEAMIS database. (For interpretation of the references to color in this figure legend, the reader is referred to the Web version of this article.)

currently limited to three index points from in situ Holocene *Porites* microatolls on the Cocos (Keeling) Islands (Woodroffe et al., 1990). The microatoll record, from which the index points have been deduced place RSL between ~0.5–1 m above msl at approximately 3 ka BP (Fig. 3c), therefore providing evidence for a RSL highstand of similar magnitude and timing as in the Central Indian Ocean (#1).

4.4. Red River Delta (#4)

Early Holocene RSL data from the southeastern coast of Vietnam comes from rotary drilling in the Red River Delta region and has been provided by Tanabe et al. (2003a), Tanabe et al. (2003b) and Hori et al. (2004). The entire dataset consists of 27 marine limiting points, mainly marine molluscs and shell fragments from prodelta deposits, eleven terrestrial limiting points containing laminated sediment samples enriched with organic material and characterized by freshwater macro- and microfossil assemblages, and seven index points interpreted as mangrove swamp deposits or intertidal mudflat accumulations (Fig. 3d). There is considerable internal data inconsistency between index and limiting points. Index points, for example, put RSL at ~ −40 m at around 10 ka BP reaching its modern position at approximately 6 ka BP. In contrast, marine limiting points places RSL at above ~ −20 m msl at 10 ka BP rising to present-day msl by about 7 ka BP.

4.5. The Sunda Shelf (#5)

4.5.1. Gulf of Thailand/South China sea (#5a)

The Gulf of Thailand/South China Sea region is characterized by a temporally well-distributed dataset of 14 marine and 41 terrestrial limiting points, and 68 index points throughout the Holocene (Somboon, 1988; Somboon and Thiramongkol, 1992; Tamura et al. 2007, 2009; Hanebuth et al., 2012; Stattegger et al., 2013). Nevertheless, the resulting age-elevation plot of reviewed RSL data for this area appear ambiguous (Fig. 3e). For example, Tamura et al. (2009) present a series of terrestrial limiting points based on massive clayey to silty deposits containing freshwater diatom assemblages and interpreted as having been deposited on a flood plain or as levee. These deposits are increasing in elevation from −15 m msl to −10 m msl between 9 and 8 ka BP (thus indicating that RSL was lower at that time). In contrast, index and marine limiting points from Somboon (1988), Somboon and Thiramongkol (1992) and Tamura et al. (2009) indicate a RSL that was substantially higher (on average −6 m msl) at that time. Allowing for some internal variability, another dataset consisting of marine limiting and index points place RSL at or slightly below modern msl between 8 and 2 ka BP (Hanebuth et al., 2012). Constraining the late Holocene history from 1 ka BP, only three RSL index points from Stattegger et al. (2013) derived from intertidal beachrock samples were found. They indicate a slightly higher-than-present RSL during the Late Holocene in the region.

4.5.2. Malay-Thai-Peninsula (#5b)

The most extensive RSL data subset comes from the central part of the Sunda Shelf, the Malay-Thai Peninsula (Fig. 3f). It comprises 79 index points, 68 terrestrial limiting and 69 marine limiting points, representing the results from 12 individual studies conducted between 1972 and 2014 (Tjia et al., 1972; Geyh et al., 1979; Tjia et al., 1983; Tjia and Fujii, 1992; Hesp et al., 1998; Scoffin and Le Tissier, 1998; Kamaludin, 2001; Horton et al., 2005; Bird et al., 2007; Bird et al., 2010; Scheffers et al., 2012; Parham et al., 2014). An almost continuous series of RSL index points (flanked by limiting points) depicts a rise of RSL from −33 m msl at 10.5 ka BP (peat from mangrove swamp; Geyh et al., 1979) to approximately present-day msl at 7 ka BP (wood from mangrove saltmarsh; Bird et al., 2007). A higher-than-present RSL is recorded by the index point data between 6 ka BP and 4 ka BP, with amplitudes between 2 m msl and 5 m msl. After 4 ka BP, RSL has been falling and likely reached msl probably during the past two millennia.

4.5.3. Java Sea (#5c)

The Java Sea RSL record is limited to two studies, both of which used fossil microatolls as RSL indicators (Azmy et al., 2010; Meltzner et al., 2017), resulting in a total of 31 index points. Index points from Azmy et al. (2010) date between 7.2 ka BP and 5.5 ka BP and indicate a RSL at about 1.5 m msl. During a similar time period, from 6.8 ka BP to 6.4 ka BP, Meltzner et al. (2017) provide index points obtained from slabbed and x-rayed fossil microatolls, showing that RSL within that timeframe fluctuated on decimeter-scales between 1.8 m and 1.2 m above msl (Fig. 3g).

4.6. Strait of Makassar (#6)

The Holocene RSL history of the Spermonde Archipelago, southwest Sulawesi, is limited to two studies (Kench and Mann, 2017) and contains 21 index points, 20 of which from fossil microatolls (Mann et al., 2016), 18 marine limiting points e.g. from bivalves such as *Anadara* sp., and unspecified oysters, and two terrestrial limiting points (de Klerk, 1982). A number of marine limiting points indicate that RSL was above present-day msl during the past 8 ka with a peak elevation at least 6.5 m above msl between approximately 6–4 ka BP (Fig. 3h). Notably, these marine limiting points contrast with the mid-Holocene microatoll record from the region that reaches a maximum elevation of ~0.2 m msl between 6 and 5 ka BP (Mann et al., 2016).

4.7. Western Tropical Pacific (#7)

Kayanne et al. (2002) provide 18 marine limiting points from massive (*Porites* sp. and *Montipora* sp.) and branching (*Acropora* sp.) corals as well as algal crusts that give minimum elevations to the RSL history of the western tropical Pacific between 8 ka BP and 2 ka BP (Fig. 3i). From this dataset, it can be deduced that RSL was above −15 m msl at 8 ka BP, reaching an elevation above −2 m msl at 6 ka BP.

4.8. Huon Peninsula (#8)

Chappell and Polach (1991) reconstructed one of the earliest RSL records from a coral drill core on uplifted reef terraces at the east coast of Huon Peninsula, Papua New Guinea. The reviewed dataset consists of 29 marine limiting points (Fig. 3j), resulting in a continuous early Holocene RSL record between 12 ka BP and 8 ka BP. During the early phase of the record, core data indicate a RSL position above −30 m msl. Core material dated to 8 ka BP indicate a continuous rise of RSL up to a position somewhere above 8 m relative to msl.

5. Discussion

The SEAMIS database shows that the broader SE Asian region experienced variable RSL histories during the Holocene. Our synthesis of RSL index points reviewed and standardized for the SEAMIS database provide records that constrain the first indicators of early Holocene sea-level rise from 12 ka BP to 8 ka BP (Figs. 2, Fig. 3a–j). After 8 ka BP, the rate of eustatic sea-level rise slowed down from approximately 9 mm/year to about 1 mm/year (Lambeck et al., 2014), with a further and possibly stepwise decrease until the onset of recent global sea-level rise some 150 years ago. It is likely that many of the index and limiting points that

are younger than 8 ka record the effects of GIA, the predominant control on RSL change in the far-field after 9–8 ka BP (Milne et al., 2005; Lambeck et al. 2010, 2014). Taking into account that the effects of GIA on RSL are spatially and temporally variable (Lambeck et al., 2002; Mitrovica and Milne, 2002), it is reasonable to expect considerable variability in the RSL records from different regions within South and SE Asia.

It is particularly apparent that the timing and magnitude of RSL highstands that occurred after 9 ka BP in the far-field are effected by GIA. When the number of RSL index and limiting points is plotted against time, ~61% occur between 9 ka BP and 6 ka BP (Fig. 3k). Looking solely at the number of index points within this time window (143 points), the percentage is even higher (67%; cf. Fig. 3l). This may imply that in most of the investigated regions, within this time window RSL was higher than present, thus leaving behind RSL samples that are more easily accessible than, for example, submerged indicators. Yet RSL data from several sub-regions of the SEAMIS database clearly show the occurrence of RSL highstands later than 6 ka BP (e.g. Woodroffe et al., 1990; Kench et al., 2009). Therefore, the prevalence of RSL data between 9 ka BP and 6 ka BP in the SEAMIS database might be a geographical artifact as the majority of RSL studies in the present database have been carried out in the Gulf of Thailand, the South China Sea and the Malay-Thai Peninsula, all regions where RSL data indicate a highstand that occurred earlier and more pronounced than on the atolls of the Indian Ocean.

There are also many instances of inconsistency between sub-regional RSL records (e.g., terrestrial limiting points lying below index or marine limiting points) in the SEAMIS database. Intrinsically contradicting results are mostly evident from the Red River Delta (#4, Fig. 3d), the Gulf of Thailand/South China Sea (#5a, Fig. 3e), the Malay-Thai-Peninsula (#5b, Fig. 3f) and the Strait of Makassar (#6, Fig. 3h). In these areas, further field studies are required to confirm whether the reported in situ indicators are instead affected by reworking or other post-formational influences on the original elevation. In the SEAMIS database, we have attempted to exclude areas with noted tectonics of variable vertical nature. However, the study area undoubtedly comprises unmapped active fault zones and the site-specific inconsistencies between RSL data within the individual sub-regions indicate that in some locations there might be a tectonic overprint. Similarly, the results of many of the studies compiled in the SEAMIS database are based on evidence from mangrove and delta deposits, both of which are environments prone to subsidence, bioturbation and compaction during sediment sampling (Brain et al. 2012, 2015). Ultimately, in the sub-regions #5a and #5b, the study sites are spread over a large area and therefore, RSL data inconsistencies in single age-elevation plots for those sub-regions might also result from the spatial variability in RSL due to GIA. In the following section, we aim to resolve possible sources of discrepancies between site-specific RSL data and identify the most robust data.

5.1. Data inconsistency assessment

5.1.1. Red River Delta (#4)

RSL data from the Red River Delta derive from three studies that describe facies variations within a number of sedimentary drill cores (Tanabe et al. 2003a, 2003b; Hori et al., 2004). In some instances, interpretations of the depositional environment are based on the presence and absence of brackish-water molluscs. For example, Unit 2 (consisting of Facies 2.1–2.3) in core ND1 of Tanabe et al. (2003a) is interpreted as having completely been deposited in a brackish-marine environment based on the occurrence of *P. amurensis* (Shrenck) and *Corbicula* sp. For the SEAMIS database, we have carefully re-interpreted sub-sections of the individual facies as marine or terrestrial limiting. Furthermore, reworking of the dated material (shells, roots and plant fragments) cannot be excluded, and delta sediments are also prone to natural subsidence over time. These processes that cause post-depositional distortions of the sedimentary sequences have not likely been adequately taken into account in the studies from the Red River Delta. Even though we included an additional uncertainty term of ±0.15 m for those samples to account for the unknown degree of compaction as suggested by Hijma et al. (2015), compaction is likely different across different coring techniques and through different sedimentary facies. This complicates the determination of the original sample position and elevation during deposition.

5.1.2. Gulf of Thailand/South China sea (#5a) and Malay-Thai-Peninsula (#5b)

In order to determine whether or not significant variations in RSL due to GIA can be expected in sub-regions #5a and #5b, we use the output of GIA models for the past 10 ka at 2-ka increments (Fig. 4). At each analyzed time step between 10 and 2 ka BP, all combinations of different model parameters considered here (see Mann et al. subm. for details) predict a significantly lower RSL in the area around the Mekong Delta in South Vietnam (Tamura et al. 2007, 2009; Hanebuth et al., 2012) than at the east coast of Vietnam (Stattegger et al., 2013) or the west coast of Thailand (Somboon, 1988; Somboon and Thiramongkol, 1992). Likewise, GIA models predict a higher RSL along the west coast of the Malay-Thai-Peninsula (Tjia et al., 1972; Geyh et al., 1979; Tjia and Fujii, 1992; Hesp et al., 1998; Scoffin and Le Tissier, 1998; Bird et al., 2007; Bird et al., 2010; Scheffers et al., 2012) than on the east coast (Tjia et al., 1983; Kamaludin, 2001; Horton et al., 2005; Parham et al., 2014). However, when the study sites are considered individually, it becomes clear that the age-elevation information for sub-region #5a is mostly inconsistent between approximately 8–6 ka BP, where numerous index points plot above terrestrial limiting points. The majority of these inconsistent RSL data stem from two studies that have been conducted around the Chao Phraya Delta in Thailand (Somboon, 1988; Somboon and Thiramongkol, 1992). The interpretation of the depositional environment in these studies is based on faunal and floral assemblages without considering the opportunity of reworking based, for example, on the recognition of shell disarticulation or a comparison with the modern pollen distribution. An additional shortcoming in these studies is that no ^{14}C laboratory code is provided, which prevents us from obtaining information on how the samples have been treated before radiocarbon dating (Millard, 2014). Such imprecise descriptions result in additional uncertainties regarding both age and elevation of RSL data that cannot be quantified.

The remaining studies from the Gulf of Thailand part of sub-region #5a (Tamura et al. 2007, 2009; Hanebuth et al., 2012) and those studies from sites susceptible to compaction within sub-region #5b (Geyh et al., 1979; Hesp et al., 1998; Kamaludin, 2001; Horton et al., 2005; Bird et al. 2007, 2010) all consider and discuss the possibilities of reworked dated material and sediment compaction. We were largely able to follow the original interpretations of intertidal index or limiting points contained in these studies. Therefore, the individual datasets themselves should be considered robust.

5.1.3. Strait of Makassar (#6)

In sub-region #6, the Strait of Makassar, marine limiting points from de Klerk (1982) plot considerably higher than the index points presented by Mann et al. (2016). In a discussion on the potential reasons for the inconsistent pattern, Mann et al. (2016) argue that the previous dataset might be less robust due to uncertainties in the IM of the implemented indicators and the lack of detail in the

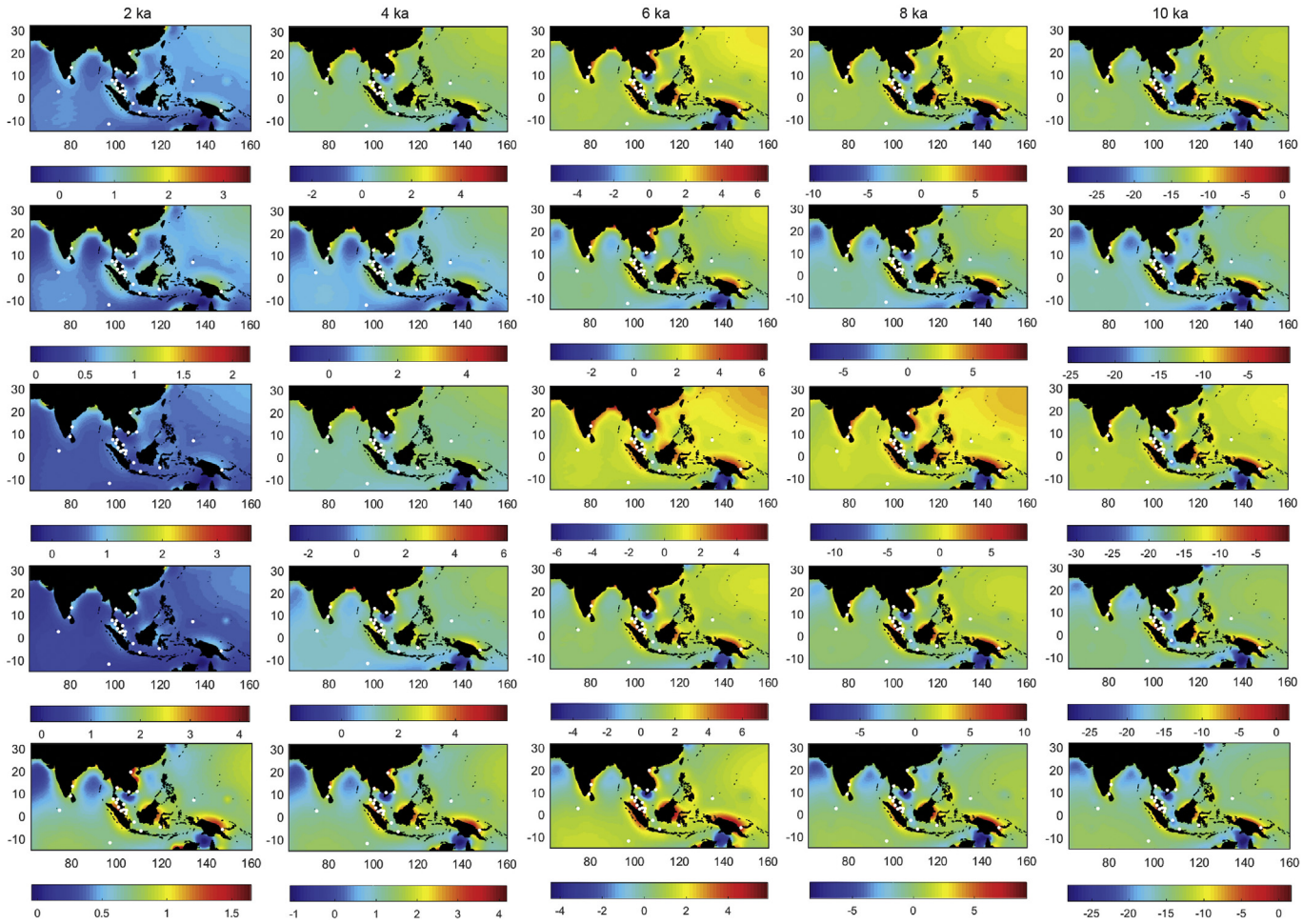

Fig. 4. RSL predictions for the broader SE Asian region between 10 ka BP and 2 ka BP based on different iterations of ice and earth models. Numbers along the left and bottom map edges indicate latitudes and longitudes. Color scales below maps indicate RSL in m relative to present-day msl. Note differences for RSL in the color values for each map. Top row: ICE5g-VM2-90 km 2nd row: ICE5g-VM2-120 km; 3rd row: ICE5g-VM2b-90km; 4th row: ICE5g-VM3-90 km; Bottom row: ICE5g-VM4-90 km. See Mann et al. (subm.) for details of simulations. (For interpretation of the references to color in this figure legend, the reader is referred to the Web version of this article.)

description of the survey methods. With regards to the offset between microatoll records from two islands in the Spermonde Archipelago, Mann et al. (2016) discuss the possibility of a localized subsidence. This assessment is based on the analysis of microatoll morphologies on the different study sites.

5.2. *Driving processes of RSL change in SE Asia, Maldives, India and Sri Lanka*

Following the discussion about possible sources for RSL data inconsistencies in the SEAMIS database, site-specific discrepancies between Tanabe et al. (2003a), Tanabe et al. (2003b) and Hori et al. (2004) (sub-region #4), Somboon (1988) and Somboon and Thiramongkol (1992) (sub-region #5a), Tjia et al. (1972) (sub-region #5b) and de Klerk (1982) and Mann et al. (2016) (sub-region #6) must be resolved with additional high-accuracy RSL data before the existing datasets can be used to decipher regional driving processes of Holocene RSL change within SE Asia. The remaining data indicate reliable RSL curves that allow assessment of driving processes of Holocene RSL change for the different sub-regions in the SEAMIS database. Moreover, the comparison between quality-controlled and tectonically corrected RSL data can potentially be used to validate model output for the suite of parameters considered here (Mann et al., subm.).

In the Central Indian Ocean, the Western Tropical Pacific, and the Huon Peninsula, the elevation of the Pleistocene unconformity underlying the Holocene reefs (Kench et al., 2009; Kayanne et al., 2002) or the last interglacial barrier reef (Chappell and Polach 1991) is commonly known. These elevations are −14.12 m msl (Central Indian Ocean; Kench et al., 2009), −15.70 m msl (Western Tropical Pacific; Kayanne et al., 2002) and +226 m msl (Huon Peninsula; Chappell and Polach, 1991). Taking into account the timing (116–129 ka BP) and most recent constraints on the position of global mean sea level (6–9 m msl) during the Last Interglacial (Dutton and Lambeck, 2012; Dutton et al., 2015), it is possible to approximate subsidence and uplift rates, and replot these three RSL records corrected accordingly (Mann et al., subm.). We remark that this is a simplified assessment, not taking into account possible perturbations to the elevation of the Last Interglacial sea level caused by GIA or mantle dynamic topography (Austermann et al., 2017).

After tectonic correction, it is instructive to see that Holocene reefs in all three study sites plot considerably lower than the GIA predictions used here. In the Central Indian Ocean, Holocene reef growth initiated at 8 ka BP when RSL (inferred from GIA modeling) was as much as 10 m above the Pleistocene unconformity. Corals continued to grow upwards with a reconstructed mean rate of reef growth of 4.7 m/ka until sea-level rise slowed and the reef reached an intertidal environment at around 6 ka BP. The reef crest core from the Western Tropical Pacific (PL-I; Kayanne et al., 2002)

similarly indicates that the Pleistocene unconformity was flooded at approximately 8 ka BP, which is comparable to the Central Indian Ocean record. Furthermore, the initiation of Holocene reef growth in the Western Tropical Pacific took place when the model-derived relative water depth accounted for 10–12 m and the mean reconstructed growth rate of corals between 8 and 6 ka BP was 6.1 m/ka. On Huon Peninsula, the corrected reef record spans from 12 to 8 ka BP and is characterized by an increasing rate of growth of 7.8 m/ka until 10 ka BP, and 15.6 m/ka from 10 to 8 ka BP and a decreasing vertical lag to modeled RSL from 20 m at 11 ka BP and 11 m at 8 ka BP.

Based on the estimated paleo-bathymetry of particular coralgal species assemblages associated with algal crust thickness, vermetid gastropods and benthic foraminifera, paleo-water depth ranges of distinct coral reef core sections can be reconstructed (Yokoyama and Esat, 2015). The reviewed coral descriptions from within the cores are limited to genus level, which prohibits us to constrain the paleo-water depth range of the dated facies to less than 10–15 m (Hibbert et al., 2016). This uncertainty precludes a coherent estimate of whether the corrected coral reef records reveal a uniform catch-up reef response during the early and middle Holocene RSL rise (Davies and Montaggioni, 1985; Neumann and Macintyre, 1985).

A number of observations regarding the driving processes of RSL change can be made from the comparison of quality-controlled RSL indicators with the modeled RSL. First, in all study sites within the SEAMIS database, the primary driving process of RSL change is GIA. This becomes especially obvious in the results from the Central Indian Ocean (Kench et al., 2009), Southeastern India (Vaz and Banerjee, 1997), the Eastern Indian Ocean (Woodroffe et al., 1990), the Malay-Thai Peninsula (Geyh et al., 1979; Hesp et al., 1998; Kamaludin, 2001) and the Java Sea (Azmy et al., 2010; Meltzner et al., 2017), where quality-controlled, tectonically corrected and internally consistent Holocene RSL index points plot significantly above the eustatic sea-level curve (Mann et al. subm.).

Second, RSL data from several studies considered in the SEAMIS database appear to be effected by syn- and post-formational sediment compaction and subsidence when compared to the modeled RSL predictions. This accounts for sites in the South China Sea (Tamura et al. 2007, 2009; Hanebuth et al., 2012) and the Malay-Thai-Peninsula (Bird et al., 2007; Bird et al., 2010; see Mann et al. subm.).

Lastly, for a few study sites, it appears that the mismatch between model output and RSL data cannot be explained by local tectonics, compaction or subsidence. For example, the Geyh et al. (1979) study indicates a RSL rise from − 22 m at 9.5 ka BP to − 2m at 8 ka BP, followed by a RSL highstand at ~5 ka BP. Here, the model likely overestimates the early Holocene RSL rise and underestimates the magnitude of the highstand (see Mann et al. subm.). The inconsistent deviations between RSL based on field evidence and modeled RSL during the early and middle Holocene suggests that for this part of the Malay-Thai Peninsula, the model output is invalid. Similarly, RSL data from microatolls in the Java Sea (Meltzner et al., 2017) show that RSL was 1.2–1.8 m above present between 6.8 and 6.4 ka BP. The models used here however do not predict a highstand at this time or of this magnitude (see Mann et al. subm.). Accordingly, additional data from these sites could be helpful to better constrain mantle viscosities for modeling sea-level change since the Last Interglacial and to better understand the Earth-Ocean-Ice system in general.

6. Conclusions

A solid understanding of the primary driving mechanisms of future RSL rise is one of the fundamental requirements for effective and sustainable coastal management on regional scales in South and SE Asia. In order to identify the processes that were responsible for Holocene RSL changes in that region, we have standardized 546 published data points in the SEAMIS database. The geographical range of the SEAMIS database stretches from the Maldives in the west to Papua New Guinea in the east, and from Vietnam in the north to Cocos (Keeling) Islands in the south. Our results show that the individual sub-regions experienced RSL histories of considerable variance. In particular a clear signal in RSL highstand variability has been detected between the Central Indian Ocean, Southeastern India, the Eastern Indian Ocean, the Malay-Thai-Peninsula, the Java Sea and the Strait of Makassar. However, neither latitudinal nor longitudinal patterns can be well constrained in the reviewed RSL data and therefore we assume that continental levering, which causes strong gradients of RSL perpendicular to the coast, is one dominant driver of the spatial variability in the magnitudes of the observed highstands.

We have furthermore identified several instances of inconsistency between grouped RSL records that do not arise from spatial variability of GIA. Following a detailed assessment of robustness we considered each data point based on the quality and RSL-related detail provided within the original sources. We then identify a number of datasets (i.e. some specific studies) that are likely responsible for the discrepancies observed. It should be noted however that the datasets are not invalid. These data meet, in the first place, the criteria for RSL index and limiting points and have accordingly been included in the SEAMIS database. It is conceivable that with more data this initial assessment on data inconsistency may change. However for the moment, we recommend end-users of the database put more weight on the consistent and quality-controlled data sets (see Mann et al. subm.).

The SEAMIS RSL data reveal that besides GIA, Holocene RSL in the region has also been affected by syn- and post-formational tectonics, compaction and subsidence. This becomes particularly evident in some sites of the central and eastern Indian Ocean, the South China Sea, the Malay-Thai-Peninsula, the Western Tropical Pacific and Huon Peninsula. However, study sites in the Strait of Malacca and the Java Sea appear to be relatively unaffected by post-formational influences. Accordingly, additional high-quality RSL data, especially from the Java Sea where little data is available so far, could be useful to calibrate competing GIA models with different eustatic history, in order to better constrain earth rheology and ice-equivalent melt-water input after 9 ka BP.

8. Author contributions

AR, TM, MV, PS and AS conceived the project; MB determined the indicative meaning for each indicator type present in the relevant literature, reviewed and standardized the published RSL data with support from AR, TM and MV; MB prepared figures with support from TM and AR; TL determined tidal datums for each geographic sub-region; PS performed GIA modeling for each geographic sub-region; TM wrote the initial manuscript that has been revised and approved by all authors.

9. Declaration of interest

The authors declare no conflict of interest.

12. Data availability

The SEAMIS database is available in a Mendeley data repository (https://doi.org/10.17632/wp4ctb4667.1). Updates to the database, netCDF files of ICE-5G model output and a MATLAB script to plot the data is accessible at https://github.com/Alerovere/SEAMIS.

Acknowledgements

This work was supported through grant SEASCHANGE (RO-5245/1-1) from the Deutsche Forschungsgemeinschaft (DFG) as part of the Special Priority Program (SPP)-1889 “Regional Sea Level Change and Society”. TM, MB, TL and AR are supported by the Leibniz Centre for Tropical Marine Research (ZMT). TL, MB and AR's research was further supported by the Institutional Strategy of the University of Bremen, funded by the German Excellence Initiative [ABPZuK-03/2014]. The authors acknowledge the working groups HOLSEA - Modelling Paleo Processes (INQUA CMP project 1601P) and PALSEA (PAGES/INQUA) for useful discussions during the 2016 workshop in Mt. Hood, Oregon. This paper also contributes to IGCP639 “Sea level change: from Minutes to Millennia”. We thank two anonymous reviewers and Glenn A. Milne for their thoughtful comments that helped to substantially improve a first draft of this paper. Thanks also to our Co-PIs and collaborators Hildegard Westphal, Benjamin P. Horton, Jamaluddin Jompa, Robert E. Kopp, Muhammad Lukman and Tilo Schöne. We furthermore thank Guest Editor Nicole Sophia Khan for her exceptional editorial support.

Appendix A. Supplementary data

Supplementary data to this article can be found online at https://doi.org/10.1016/j.quascirev.2019.07.007.

References

Armitage, S.J., Jasim, S.A., Marks, A.E., Parker, A.G., Usik, V.I., Uerpmann, H.-P., 2011. The southern route “out of Africa”: Evidence for an early expansion of modern humans into Arabia. Science 331 (6016), 453 LP-456.

Austermann, J., Mitrovica, J.X., Huybers, P., Rovere, A., 2017. Detection of a dynamic topography signal in last interglacial sea-level records. Sci. Adv. 3 (7), e1700457.

Azmy, K., Edinger, E., Lundberg, J., Diegor, W., 2010. Sea level and paleotemperature records from a mid-Holocene reef on the North coast of Java, Indonesia. Int. J. Earth Sci. 99 (1), 231–244. https://doi.org/10.1007/s00531-008-0383-3.

Banerjee, P.K., 2000. Holocene and Late Pleistocene relative sea level fluctuations along the east coast of India. Mar. Geol. 167 (3–4), 243–260. https://doi.org/10.1016/S0025-3227(00)00028-1.

Bird, P., 2003. An updated digital model of plate boundaries. Geochem. Geophys. Geosyst. https://doi.org/10.1029/2001GC000252.

Bird, M.I., Fifield, L.K., Teh, T.S., Chang, C.H., Shirlaw, N., Lambeck, K., 2007. An inflection in the rate of early mid-Holocene eustatic sea-level rise: A new sea-level curve from Singapore. Estuar. Coast Shelf Sci. 71 (3–4), 523–536. https://doi.org/10.1016/j.ecss.2006.07.004.

Bird, M.I., Austin, W.E.N., Wurster, C.M., Fifield, L.K., Mojtahid, M., Sargeant, C., 2010. Punctuated eustatic sea-level rise in the early mid-Holocene. Geology. https://doi.org/10.1130/G31066.1.

Bloom, A.L., 1977. Atlas of Sea Level Curves. International Geological Correlation Program, Project 16. Cornell University. Geology Department, Ithaca, NY.

Bradley, S.L., Milne, G.A., Horton, B.P., Zong, Y., 2016. Modelling sea level data from China and Malay-Thailand to estimate Holocene ice-volume equivalent sea level change. Quat. Sci. Rev. 137, 54–68.

Brain, M.J., Long, A.J., Woodroffe, S.A., Petley, D.N., Milledge, D.G., Parnell, A.C., 2012. Modelling the effects of sediment compaction on salt marsh reconstructions of recent sea-level rise. Earth Planet. Sci. Lett. 345, 180–193.

Brain, M.J., Kemp, A.C., Horton, B.P., Culver, S.J., Parnell, A.C., Cahill, N., 2015. Quantifying the contribution of sediment compaction to late Holocene salt-marsh sea-level reconstructions, North Carolina, USA. Quat. Res. 83 (1), 41–51.

Carto, S.L., Weaver, A.J., Hetherington, R., Lam, Y., Wiebe, E.C., 2009. Out of Africa and into an ice age: On the role of global climate change in the late Pleistocene migration of early modern humans out of Africa. J. Hum. Evol. 56 (2), 139–151. https://doi.org/10.1016/j.jhevol.2008.09.004.

Cazenave, A., Cozannet, G. Le, 2013. Sea level rise and its coastal impacts. Earth's Future 2, 15–34. https://doi.org/10.1002/2013EF000188.Received.

Chappell, J., Polach, H., 1991. Post-glacial sea-level rise from a coral record at Huon Peninsula, Papua New Guinea. Nature 349 (6305), 147–149. https://doi.org/10.1038/349147a0.

Chaussard, E., Amelung, F., Abidin, H., Hong, S.H., 2013. Sinking cities in Indonesia: ALOS PALSAR detects rapid subsidence due to groundwater and gas extraction. Remote Sens. Environ. 128, 150–161. https://doi.org/10.1016/j.rse.2012.10.015.

Darman, H., Sidi, F.H., 2000. An Outline of the Geology of Indonesia. Indonesian Association of Geologists, Jakarta, p. 192.

Davies, P.J., Montaggioni, L., 1985. Reef growth and sea-level change: The environmental signature. In: Proceedings 5th International Coral Reef Congress, Tahiti, pp. 477–511.

de Klerk, L.G., 1982. Zeespiegels, riffen en kustvlakten in zuidwest Sulawesi, Indonesië: een morfogenetisch-bodemkundige studie. Geografisch Instituut, Rijksuniversiteit Utrecht.

Dutton, A., Lambeck, K., 2012. Ice Volume and Sea Level during, vol. 216, pp. 216–220. https://doi.org/10.1126/science.1205749. July.

Dutton, A., Carlson, A.E., Long, A.J., Milne, G.A., Clark, P.U., DeConto, R., Horton, B.P., Rahmstorf, S., Raymo, M.E., 2015. Sea-level rise due to polar ice-sheet mass loss during past warm periods. Science 349 (6244). https://doi.org/10.1126/science.aaa4019.

Egbert, G.D., Erofeeva, S.Y., 2002. Efficient inverse modeling of barotropic ocean tides. J. Atmos. Ocean. Technol. 19 (2), 183–204.

Engelhart, S.E., Horton, B.P., 2012. Holocene sea level database for the Atlantic coast of the United States. Quat. Sci. Rev. 54, 12–25. https://doi.org/10.1016/j.quascirev.2011.09.013.

Engelhart, S.E., Horton, B.P., Roberts, D.H., Bryant, C.L., Corbett, D.R., 2007. Mangrove pollen of Indonesia and its suitability as a sea-level indicator. Mar. Geol. 242 (1–3), 65–81.

Engelhart, S.E., Peltier, W.R., Horton, B.P., 2011. Holocene relative sea-level changes and glacial isostatic adjustment of the U.S. Atlantic coast. Geology 39 (8), 751–754. https://doi.org/10.1130/G31857.1.

Engelhart, S.E., Vacchi, M., Horton, B.P., Nelson, A.R., Kopp, R.E., 2015. A sea-level database for the Pacific coast of central North America. Quat. Sci. Rev. 113, 78–92. https://doi.org/10.1016/j.quascirev.2014.12.001.

Fontana, A., Vinci, G., Tasca, G., Mozzi, P., Vacchi, M., Bivi, G., Salvador, S., Rossato, S., Antonioli, F., Asioli, A., 2017. Lagoonal settlements and relative sea level during Bronze Age in Northern Adriatic: Geoarchaeological evidence and paleogeographic constraints. Quat. Int. 439, 17–36.

Gehrels, R., Long, A., 2008. Sea level is not level. Geography 93 (Part 1).

Geyh, M.A., Kudrass, H.R., Streif, H., 1979. sea-level changes during the late Pleistocene and Holocene in the Strait of Malacca. Nature 278, 441–443.

Hall, R., Blundell, D.J., 1996. Tectonic Evolution of SE Asia: Introduction. Geological Society of London.

Hall, R., Spakman, W., 2015. Mantle structure and tectonic history of SE Asia. Tectonophysics 658, 14–45.

Hanebuth, T., Stattegger, K., G, P. M, 2000. Rapid Flooding of the Sunda shelf: A late glacial sea level record. Science 288 (May), 1033–1035. https://doi.org/10.1126/science.288.5468.1033.

Hanebuth, T.J.J., Voris, H.K., Yokoyama, Y., Saito, Y., Okuno, J., 2011. Formation and fate of sedimentary depocentres on Southeast Asia's Sunda Shelf over the past sea-level cycle and biogeographic implications. Earth Sci. Rev. 104 (1–3), 92–110. https://doi.org/10.1016/j.earscirev.2010.09.006.

Hanebuth, T.J.J., Proske, U., Saito, Y., Nguyen, V.L., Ta, T.K.O., 2012. Early growth stage of a large delta—Transformation from estuarine-platform to deltaic-progradational conditions (the northeastern Mekong River Delta, Vietnam). Sediment. Geol. 261, 108–119.

Hanson, S., Nicholls, R., Ranger, N., Hallegatte, S., Corfee-Morlot, J., Herweijer, C., Chateau, J., 2011. A global ranking of port cities with high exposure to climate extremes. Clim. Change. https://doi.org/10.1007/s10584-010-9977-4.

Hesp, P.A., Hung, C.C., Hilton, M., Ming, C.L., Turner, I.M., 1998. A first tentative Holocene sea-level curve for Singapore. J. Coast. Res. 308–314.

Hibbert, F.D., Rohling, E.J., Dutton, A., Williams, F.H., Chutcharavan, P.M., Zhao, C., Tamisiea, M.E., 2016. Coral indicators of past sea-level change: A global repository of U-series dated benchmarks. Quat. Sci. Rev. 145, 1–56. https://doi.org/10.1016/J.QUASCIREV.2016.04.019.

Hijma, M.P., Cohen, K.M., 2010. Timing and magnitude of the sea-level jump preluding the 8200 yr event. Geology 38 (3), 275–278.

Hijma, M.P., Engelhart, S.E., Törnqvist, T.E., Horton, B.P., Hu, P., Hill, D.F., 2015. A protocol for a geological sea-level database. In: Shennan, I., Long, A.J., Horton, B.P. (Eds.), Handbook of Sea-Level Research. Wiley Online Library, pp. 536–553.

Hopley, D., Gehrels, R., 2007. Holocene Sea-Level Research and IGCP – the Last 40 Years, 1986.

Hori, K., Tanabe, S., Saito, Y., Haruyama, S., Nguyen, V., Kitamura, A., 2004. Delta initiation and Holocene sea-level change: Example from the Song Hong (Red River) delta, Vietnam. Sediment. Geol. 164 (3–4), 237–249.

Horton, B.P., Gibbard, P.L., Milne, G.M., Morley, R.J., Purintavaragul5, C., Stargardt, J.M., 2005. Holocene sea levels and palaeoenvironments, Malay-Thai Peninsula, southeast Asia. Holocene 158, 1199–1213.

Horton, B.P., Zong, Y., Hillier, C., Engelhart, S., 2007. Diatoms from Indonesian mangroves and their suitability as sea-level indicators for tropical environments. Mar. Micropaleontol. 63, 155–168. https://doi.org/10.1016/j.marmicro.2006.11.005.

Horton, B.P., Peltier, W.R., Culver, S.J., Drummond, R., Engelhart, S.E., Kemp, A.C., Mallinson, D., Thieler, E.R., Riggs, S.R., Ames, D.V., 2009. Holocene sea-level changes along the North Carolina Coastline and their implications for glacial isostatic adjustment models. Quat. Sci. Rev. 28 (17–18), 1725–1736.

Horton, B.P., Engelhart, S.E., Hill, D.F., Kemp, A.C., Nikitina, D., Miller, K.G., Peltier, W.R., 2013. Influence of tidal-range change and sediment compaction on Holocene relative sea-level change in New Jersey, USA. J. Quat. Sci. 28 (4), 403–411.

Kamaludin, H.B., 2001. Holocene Sea Level Changes in Kelang and Kuantan, Peninsular Malaysia. Durham University. Retrieved from. http://etheses.dur.ac.uk/3786/.

Kayanne, H., Yamamo, H., Randall, R.H., 2002. Holocene sea-level changes and barrier reef formation on an oceanic island, Palau Islands, western pacific.

Sediment. Geol. 150, 47–60.
Kench, P.S., Mann, T., 2017. Reef island evolution and dynamics: Insights from the Indian and pacific oceans and Perspectives for the Spermonde archipelago. Front. Mar. Sci. 4 (May) https://doi.org/10.3389/fmars.2017.00145.
Kench, P.S., Smithers, S.G., McLean, R.F., Nichol, S.L., 2009. Holocene reef growth in the Maldives: Evidence of a mid-Holocene sea-level highstand in the central Indian Ocean. Geology 37 (5), 455–458. https://doi.org/10.1130/G25590A.1.
Lambeck, K., Chappell, J., 2001. Sea level change through the last glacial cycle. Science (New York, N.Y.) 292 (5517), 679–686. https://doi.org/10.1126/science.1059549.
Lambeck, K., Esat, T.M., Potter, E.-K., 2002. Links between climate and sea levels for the past three million years. Nature 419 (6903), 199.
Lambeck, K., Woodroffe, C.D., Antonioli, F., Anzidei, M., Gehrels, W.R., Laborel, J., Wright, A.J., 2010. Paleoenvironmental Records, Geophysical Modelling, and Reconstruction of Sea Level Trends and Variability on Centennial and Longer Timescales. Understanding sea level rise and variability. Wiley-Blackwell.
Lambeck, K., Rouby, H., Purcell, A., Sun, Y., Sambridge, M., 2014. sea Level and global ice volumes from the last glacial maximum to the Holocene. Proc. Natl. Acad. Sci. Unit. States Am. https://doi.org/10.1073/pnas.1411762111.
Long, A.J., Roberts, D.H., Dawson, S., 2006. Early Holocene history of the West Greenland ice sheet and the GH-8.2 event. Quat. Sci. Rev. 25 (9–10), 904–922.
Love, R., Milne, G.A., Tarasov, L., Engelhart, S.E., Hijma, M.P., Latychev, K., Horton, B.P., Törnqvist, T.E., 2016. The contribution of glacial isostatic adjustment to projections of sea-level change along the Atlantic and Gulf coasts of North America. Earth's Future 4, 440–464. https://doi.org/10.1002/2016EF000363.Received.
Mann, T., Bender, M., Lorscheid, T., Stocchi, P., Vacchi, M., Switzer, A., & Rovere, A. (subm.). Relative sea-level data from the SEAMIS database compared to ICE-5G model predictions of glacial isostatic adjustment. Data in Brief.
Mann, T., Rovere, A., Schöne, T., Klicpera, A., Stocchi, P., Lukman, M., Westphal, H., 2016. The magnitude of a mid-Holocene sea-level highstand in the Strait of Makassar. Geomorphology 257, 155–163. https://doi.org/10.1016/j.geomorph.2015.12.023.
Mauz, B., Vacchi, M., Green, A., Hoffmann, G., Cooper, A., 2015. Beachrock: A tool for reconstructing relative sea level in the far-field. Mar. Geol. https://doi.org/10.1016/j.margeo.2015.01.009.
McCaffrey, R., 1996. Slip partitioning at convergent plate boundaries of SE Asia. Geol. Soc. Lond Spec. Publ. 106 (1), 3–18.
Melis, R.T., Di Rita, F., French, C., Marriner, N., Montis, F., Serreli, G., Sulas, F., Vacchi, M., 2018. 8000 years of coastal changes on a western Mediterranean island: A multiproxy approach from the Posada plain of Sardinia. Mar. Geol. 403, 93–108.
Meltzner, A.J., Woodroffe, C.D., 2015. Coral microatolls. Handb. Sea Level Res. 125–145.
Meltzner, A.J., Switzer, A.D., Horton, B.P., Ashe, E., Qiu, Q., Hill, D.F., Bradley, S.L., Kopp, R.E., Hill, E.M., Majewski, J.M., Natawidjaja, D.H., Suwargadi, B.W., 2017. Half-metre sea-level fluctuations on centennial timescales from mid-Holocene corals of Southeast Asia. Nat. Commun. 8 https://doi.org/10.1038/ncomms14387.
Michelli, M., 2008. Sea-level Changes, Coastal Evolution and Paleoceanography of Coastal Waters in SE-Vietnam since the Mid-holocene.
Millard, A.R., 2014. Conventions for reporting radiocarbon determinations. Radiocarbon 56 (02), 555–559. https://doi.org/10.2458/56.17455.
Milne, G.A., Long, A.J., Bassett, S.E., 2005. Modelling Holocene relative sea-level observations from the Caribbean and south America. Quat. Sci. Rev. 24 (10–11), 1183–1202.
Mitrovica, J.X., Milne, G.A., 2002. On the origin of late Holocene sea-level highstands within equatorial ocean basins. Quat. Sci. Rev. 21 (20–22), 2179–2190. https://doi.org/10.1016/S0277-3791(02)00080-X.
Mitrovica, J.X., Peltier, W.R., 1991. On postglacial geoid subsidence over the equatorial oceans. J. Geophys. Res.: Solid Earth 96 (B12), 20053–20071.
Murray-Wallace, C.V., Scott, D.B., 1999. Late quaternary coastal records of rapid change: Application to present and future conditions (IGCP Project 367). Quat. Int. 56, 1–154.
Neumann, A.C., Macintyre, I., 1985. Reef response to sea level rise: Keep-up, catch-up or give up. In: Proceedings 5th International Coral Reef Congress, Tahiti, pp. 105–110.
Nicholls, R.J., Cazenave, A., 2010. Sea-level rise and its impact on coastal zones. Science. https://doi.org/10.1126/science.1185782.
Parham, P.R., Saito, Y., Sapon, N., Suriadi, R., Mohtar, N.A., 2014. Evidence for ca. 7-ka maximum Holocene transgression on the Peninsular Malaysia east coast. J. Quat. Sci. https://doi.org/10.1002/jqs.2714.
Peltier, W.R., 1999. Global sea level rise and glacial isostatic adjustment. Glob. Planet. Chang. 20 (2–3), 93–123.
Pluet, J., Pirazzoli, P.A., 1991. World Atlas of Holocene Sea-Level Changes, vol. 58. Elsevier.
Preuss, H., 1979. Progress in computer evaluation of sea level data within the IGCP Project no. 61. In: Proceedings of the 1978 International Symposium of Coastal Evolution in the Quaternary, Sao Paulo, Brazil, pp. 104–134.
Reimer, P.J., Bard, E., Bayliss, A., Beck, J.W., Blackwell, P.G., Ramsey, C.B., Buck, C.E., Cheng, H., Edwards, R.L., Friedrich, M., 2013. IntCal13 and Marine13 radiocarbon age calibration curves 0–50,000 years cal BP. Radiocarbon 55 (4), 1869–1887.
Rovere, A., Antonioli, F., Bianchi, C.N., 2015. Fixed biological indicators. In: Shennan, I., Long, A.J., Horton, B.P. (Eds.), Handbook of Sea-Level Research. Wiley Online Library, pp. 268–280.
Roy, K., Peltier, W.R., 2015. Glacial isostatic adjustment, relative sea level history and mantle viscosity: Reconciling relative sea level model predictions for the US East coast with geological constraints. Geophys. J. Int. 201 (2), 1156–1181.
Sarr, A.C., Husson, L., Sepulchre, P., Pastier, A.M., Pedoja, K., Elliot, M., Arias-Ruiz, C., Solihuddin, T., Aribowo, S., Susilohadi, 2019. Subsiding Sundaland. Geology 47 (2), 119–122.
Scheffers, A., Brill, D., Kelletat, D., Brückner, H., Scheffers, S., Fox, K., 2012. Holocene sea levels along the Andaman Sea coast of Thailand. Holocene 22 (10), 1169–1180. https://doi.org/10.1177/0959683612441803.
Scoffin, T.P., Le Tissier, M.D.A., 1998. Late Holocene sea level and reef-flat progradation, Phuket, South Thailand. Coral Reefs 17 (3), 273–276. https://doi.org/10.1007/s003380050128.
Scoffin, T.P., Stoddart, D.R., 1978. The nature and significance of microatolls. Phil. Trans. Roy. Soc. Lond. B Biol. Sci. 284 (999), 99–122.
Shennan, I., 1992. Quaternary coastal evolution: Case studies, models and regional patterns. In: Proc. Of the Geologists' Assoc., vol. 103. Geol. soc. publ. house Bath.
Shennan, I., Horton, B., 2002. Holocene land-and sea-level changes in Great Britain. J. Quat. Sci.: Publ. Quat. Res. Assoc. 17 (5-6), 511–526.
Shennan, I., Long, A.J., Horton, B.P., 2015. Handbook of Sea-Level Research. John Wiley & Sons.
Sieh, K., Natawidjaja, D.H., Meltzner, A.J., Shen, C.-C., Cheng, H., Li, K.-S., Suwargadi, B.W., Galetzka, J., Philibosian, B., Edwards, R.L., 2008. Earthquake supercycles inferred from sea-level changes recorded in the corals of west Sumatra. Science 322 (5908), 1674–1678.
Simandjuntak, T.O., Barber, A.J., 1996. Contrasting tectonic styles in the Neogene orogenic belts of Indonesia. Geol. Soc. Lond Spec. Publ. 106 (1), 185–201.
Simons, W.J.F., Socquet, A., Vigny, C., Ambrosius, B.A.C., Haji Abu, S., Promthong, C., Subarya, C., Sarsito, D.A., Matheussen, S., Morgan, P., 2007. A decade of GPS in Southeast Asia: Resolving Sundaland motion and boundaries. J. Geophys. Res.: Solid Earth 112 (B6).
Smithers, S.G., Woodroffe, C.D., 2000. Microatolls as sea-level indicators on a mid-ocean atoll. Mar. Geol. 168 (1–4), 61–78. https://doi.org/10.1016/S0025-3227(00)00043-8.
Somboon, J.R.P., 1988. Paleontological study of the recent marine sediments in the lower central plain, Thailand. J. Southeast Asian Earth Sci. 2 (3–4), 201–210. https://doi.org/10.1016/0743-9547(88)90031-1.
Somboon, J.R.P., Thiramongkol, N., 1992. Holocene highstand shoreline of the Chao Phraya delta, Thailand. J. Southeast Asian Earth Sci. 7 (1), 53–60. https://doi.org/10.1016/0743-9547(92)90014-3.
Southon, J., Kashgarian, M., Fontugne, M., Metivier, B., Yim, W.W.S., 2002. Marine reservoir corrections for the Indian ocean and Southeast Asia. Radiocarbon 44 (1), 167–180.
Stattegger, K., Tjallingii, R., Saito, Y., Michelli, M., Trung Thanh, N., Wetzel, A., 2013. Mid to late Holocene sea-level reconstruction of Southeast Vietnam using beachrock and beach-ridge deposits. Glob. Planet. Chang. 110, 214–222. https://doi.org/10.1016/j.gloplacha.2013.08.014.
Stuiver, M., Polach, H.A., 1977. Discussion reporting of 14 C data. Radiocarbon 19 (3), 355–363.
Switzer, A.D., Sloss, C.R., Horton, B.P., Zong, Y., 2012. Preparing for coastal change. Quat. Sci. Rev. 54, 1–3.
Tam, C.Y., Zong, Y., bin Hassan, K., bin Ismal, H., binti Jamil, H., Xiong, H., Wu, P., Sun, Y., Huang, G., Zheng, Z., 2018. A below-the-present late Holocene relative sea level and the glacial isostatic adjustment during the Holocene in the Malay Peninsula. Quat. Sci. Rev. 201, 206–222.
Tamura, T., Saito, Y., Sieng, S., Ben, B., Kong, M., Choup, S., Tsukawaki, S., 2007. Depositional facies and radiocarbon ages of a drill core from the Mekong River lowland near Phnom Penh, Cambodia: Evidence for tidal sedimentation at the time of Holocene maximum flooding. J. Asian Earth Sci. 29 (5–6), 585–592. https://doi.org/10.1016/j.jseaes.2006.03.009.
Tamura, T., Saito, Y., Sieng, S., Ben, B., Kong, M., Sim, I., Choup, S., Akiba, F., 2009. Initiation of the Mekong River delta at 8 ka: Evidence from the sedimentary succession in the Cambodian lowland. Quat. Sci. Rev. 28 (3–4), 327–344.
Tanabe, S., Hori, K., Saito, Y., Haruyama, S., Sato, Y., Hiraide, S., 2003a. Sedimentary facies and radiocarbon dates of the Nam Dinh-1 core from the Song Hong (Red River) delta, Vietnam. J. Asian Earth Sci. 21 (5), 503–513.
Tanabe, S., Hori, K., Saito, Y., Haruyama, S., Kitamura, A., 2003b. Song Hong (Red River) delta evolution related to millennium-scale Holocene sea-level changes. Quat. Sci. Rev. 22 (21–22), 2345–2361.
Tjia, H.D., 1996. Sea-level changes in the tectonically stable Malay-Thai Peninsula. Quat. Int. 31, 95–101. https://doi.org/10.1016/1040-6182(95)00025-E.
Tjia, H.D., Fujii, S., 1992. Late Quaternary Shoreline in Peningsular Malaysia.
Tjia, H.D., Liew, K.K., 1996. Changes in tectonic stress field in northern Sunda Shelf basins. Geol. Soc. Lond Spec. Publ. 106 (1), 291–306.
Tjia, H.D., Fujii, S., Kigoshi, K., Sugimura, A., Zakaria, T., 1972. Radiocarbon dates of elevated shorelines, Indonesia and Malaysia. Part 1. Quat. Res. https://doi.org/10.1016/0033-5894(72)90087-7.
Tjia, H.D., Fujii, S., Kigoshi, K., 1983. Holocene shorelines of Tioman island in the south China sea. In: Terwindt, J., J. H, Van Steijn, H. (Eds.), Developments in Physical Geogrqphy - a Tribute to J. I. S. Zonneveld, pp. 599–604.
Törnqvist, T.E., González, J.L., Newsom, L.A., Van der Borg, K., De Jong, A.F.M., Kurnik, C.W., 2004. Deciphering Holocene sea-level history on the US Gulf coast: A high-resolution record from the Mississippi delta. Geol. Soc. Am. Bull. 116 (7–8), 1026–1039.
Törnqvist, T.E., Rosenheim, B.E., Hu, P., Fernandez, A.B., 2015. Radiocarbon dating and calibration. In: Shennan, I., Long, A.J., Horton, B.P. (Eds.), Handbook of Sea-

Level Research, pp. 349–360.
Vacchi, M., Marriner, N., Morhange, C., Spada, G., Fontana, A., Rovere, A., 2016. Multiproxy assessment of Holocene relative sea-level changes in the western Mediterranean: Sea-level variability and improvements in the definition of the isostatic signal. Earth Sci. Rev. 155, 172–197.
van de Plassche, O., 1982. Sea-level Change and Water-Level Movements in the Netherlands during the Holocene. Ph. D. dissertation. Vrije Universiteit, Amsterdam.
Van de Plassche, O., 1986. Sea-level Research: A Manual for the Collection Andevaluation of Data. Springer.
Vaz, G.G., Banerjee, P.K., 1997. Middle and late Holocene sea level changes in and around Pulicat Lagoon, Bay of Bengal, India. Mar. Geol. 138 (3–4), 261–271. https://doi.org/10.1016/S0025-3227(97)00008-X.
Woodroffe, S.A., Horton, B.P., 2005. Holocene sea-level changes in the Indo-Pacific. J. Asian Earth Sci. https://doi.org/10.1016/j.jseaes.2004.01.009.
Woodroffe, C., McLean, R., Polach, H., Wallensky, E., 1990. Sea level and coral atolls: Late Holocene emergence in the Indian Ocean. Geology 18 (1), 62–66. 10.1130/0091-7613(1990)018<0062:SLACAL>2.3.CO;2.
Woodroffe, C.D., McGregor, H.V., Lambeck, K., Smithers, S.G., Fink, D., 2012. Mid-Pacific microatolls record sea-level stability over the past 5000 yr. Geology 40 (10), 951–954. https://doi.org/10.1130/G33344.1.
Yokoyama, Y., Esat, T.M., 2015. Coral reefs. In: Handbook of Sea-Level Research. John Wiley & Sons, Ltd, Chichester, UK, pp. 104–124. https://doi.org/10.1002/9781118452547.ch7.
Yokoyama, Y., Esat, T.M., Thompson, W.G., Thomas, A.L., Webster, J.M., Miyairi, Y., Sawada, C., Aze, T., Matsuzaki, H., Okuno, J., Fallon, S., Braga, J.-C., Humblet, M., Iryu, Y., Potts, D.C., Fujita, K., Suzuki, A., Kan, H., 2018. Rapid glaciation and a two-step sea level plunge into the Last Glacial Maximum. Nature 559 (7715), 603–607. https://doi.org/10.1038/s41586-018-0335-4.
Yousefi, M., Milne, G.A., Love, R., Tarasov, L., 2018. Glacial isostatic adjustment along the Pacific coast of central North America. Quat. Sci. Rev. 193, 288–311. https://doi.org/10.1016/J.QUASCIREV.2018.06.017.